Preceding winter La Niña reduces Indian summer monsoon rainfall

Environmental Research Letters

LETTER

Preceding winter La Niña reduces Indian summer monsoon rainfall

Arindam Chakraborty

Centre for Atmospheric and Oceanic Sciences, and Divecha Centre for Climate Change, Indian Institute of Science, Bangalore 560012, India

E-mail: arch@iisc.ac.in

OPEN ACCESS

RECEIVED
12 November 2017

REVISED
1 April 2018

ACCEPTED FOR PUBLICATION
12 April 2018

PUBLISHED
14 May 2018

Keywords: Indian summer monsoon droughts, winter La Niña, moisture flux, global delayed teleconnection

Supplementary material for this article is available online

Abstract

Leaving out the strong El Niño Southern Oscillation (ENSO) years, our understanding in the interannual variation of the Indian summer monsoon rainfall (ISMR) stands poor for the rest. This study quantifies the role of ENSO in the preceding winter on ISMR with a particular emphasis on ENSO-neutral summer and La Niña winter. Results show that, unlike the simultaneous ENSO-ISMR relationship, La Niña of previous winter reduces mean rainfall over the country by about 4% even during ENSO neutral summer. Moreover, when ENSO changes phase from La Niña in winter to El Niño in summer, ISMR is anomalously lower than during persisting El Niño years (−14.5% and −5.3%, respectively), increasing the probability of severe drought. This suppression effect of La Niña of the preceding winter on summer monsoon precipitation over India is mostly experienced in its western and southern parts. Principal component analysis of the zonal propagation of surface pressure anomalies from winter to summer along Northern Hemisphere subtropics decomposes interannual variations of seasonally persisting anomalies from zonal propagations. The dominant modes are associated with the seasonal transition of the ENSO phase, and are well correlated with date of onset and seasonal mean rainfall of monsoon over India. These results improve our understanding of the interannual variations of ISMR and could be used for diagnostics of general circulation models.

1. Introduction

The interannual variation of Indian summer monsoon rainfall (ISMR) bears crucial socio-economic values to the country of teeming millions [1, 2]. ISMR exhibits quasi-periodicity at time periods from biennial to multi-decadal [3]. The identification of the physical mechanism driving this interannual variation would not only provide a pathway to improve the seasonal prediction of ISMR, but is also central to understanding organized tropical convection and associated interaction with the non-linear, transient global climate [4–7].

The gigantic circulation of the Asian summer monsoon [8, 9], of which the Indian monsoon is a part, shows notable east-west asymmetry at lead zonal wave-number. It is known that the El Niño Southern Oscillation (ENSO) impacts ISMR by controlling the strength and position of this circulation [10, 11]. ENSO could also impact ISMR through modulation of the stationary Rossby wave of the midlatitude [12, 13]. On the other hand, the strength of Indian monsoon in summer (weak or strong) skews the probability of development of El Niño or La Niña in the following winter [14, 15]. Such interactions have associated time scales that control the lagged response between components of the system.

This time-lag in response between the ENSO and Asian monsoon, combined with the seasonality of their phases, is possibly the key to explaining the observed asymmetry in the East Asian summer monsoon between the developing and decaying phases of ENSO [16–18], and its dependence on the mean state of climate [19]. It has been shown that the decaying (developing) mean sea level pressure of Darwin from winter to spring increases (decreases) the following ISMR [20]. This was used, in conjunction with other parameters, to develop a statistical prediction model for

ISMR [21]. Tendencies of eastern Pacific sea surface temperature (SST) are also used for the real-time prediction of ISMR [22] using the statistical model. However, the skill of such models could vary on decadal time scales depending on the mean state [23, 24].

Although there are several studies addressing the importance of the change of phase of ENSO on the East Asian monsoon [16, 25, 19], such quantifications are limited for Indian summer monsoon. This is especially important for the ENSO neutral summer for which identification of an exact reason for the spatial distribution of precipitation anomalies over India has been elusive. This study quantifies the changing footprint of ENSO from winter to summer on ISMR with special emphasis on the ENSO neutral summer. It also puts forward a mechanism that can explain the observed delayed response of ISMR to winter ENSO conditions.

2. Methods

We use precipitation data sets from two different sources. The first one is a 144 year long record of raingauge-based precipitation over India [26], available from 1871 through 2014. We also use raingauge-based precipitation at every $1^\circ \times 1^\circ$ grid over India, obtained from the India Meteorological Department (IMD), available as daily averages from 1901 through 2014 [27].

We use Hadley Centre Interpolated SST observations [28], available at global regular grids, monthly averages from 1870 through present. Monthly mean atmospheric parameters such as surface pressure (p_s), winds and humidity were taken from the National Center for Environmental Prediction /National Center for Atmospheric Research (NCEP/NCAR) Reanalysis 1 (R1). This data is available from 1948 through present [29].

In this study ISMR is defined as June–September mean area averaged precipitation over India, as in [26]. Prior to any calculation, anomalies were created removing the monthly mean annual cycle from all data sets. We average SST of Nino 3.4 region (190°–240°E, 5°S–5°N; termed as *N34SST* henceforth) during Northern Hemispheric summer (June–September: JJAS) and the preceding winter (December–February; DJF) to categorize them into phases of ENSO. If N34SST is less than −0.5°C (greater than 0.5°C), we identify that season as La Niña (El Niño), the rest being ENSO neutral. Owing to the slowly varying nature of N34SST, such definitions of ENSO using four (June–September) and three (December–February) months averages is close to the definition of ENSO that uses three month running average (supplementary table S1 available at stacks.iop.org/ERL/13/054030/mmedia). In this study, we identify years into nine possible categories: from DJF La Niña, neutral or El Niño to JJAS La Niña, neutral or El Niño. List of these years from 1871 through 2014 are provided in supplementary table S2. The corresponding composites of N34SST from December through September are shown in figure S1. While using a shorter length data set, we use the corresponding subset from this list.

Vertically integrated moisture flux is calculated at every grid of R1 using standard procedure.

To understand interannual modes of time-longitude evolution of p_s, principal component (PC) analysis is performed on the 20°–30°N mean p_s anomalies from January through September.

$$p_s(X, M, T) = \sum_{n=1}^{N} \phi_n(X, M)\, \tau_n(T) \qquad (1)$$

where $p_s(X, M, T)$ is surface pressure anomaly averaged along 20°–30°N. ϕ_n and τ_n are the nth empirical orthogonal function (EOF) pattern and PC time series, respectively. X is number of longitude grids (144 for R1). M is number of months (January–September: nine). T is number of years. N is number of PCs. In other words, we replace the traditional 'space' (longitude–latitude) of standard PC analysis with Hovmoller (longitude–month) patterns. The time T is interannual variations of this pattern (1948 through 2014: 67 years).

The date of the onset of monsoon over Kerala (MoK) was calculated using daily rainfall averaged between 74°–78°E, 8°–12°N, and vertically integrated (surface to 600 hPa) zonal wind averaged between 55°–75°E, 5°–12.5°N. The MoK is defined as the first day of the monsoon season (after 15 May) when the rainfall exceeds 4 mm d^{-1} and remains above this value for at least three consecutive days, and the zonal wind is above 3 m s^{-1} for at least ten consecutive days. This definition is same as that in [30].

We do not remove any long-term trend from any data set. Results, especially those involve computation of spatial pattern, are dependent on the method used for trend removal [31]. This is because it is possible to modify some real modes/oscillations by removing a trend from a short time series. Moreover, the observed trend of N34SST, which is the focus of this study, is weak. Despite this, please note that the identified years in all nine categories (supplementary table S2) are evenly distributed along the 144 year timeline.

3. Results

A scatter plot between N34SST in JJAS and ISMR reconfirms their general out-of-phase relationship (figure 1(*a*)). The linear correlation coefficient is −0.57, suggesting that N34SST in JJAS is associated with 32.5% of the total interannual variance of ISMR. While most of the La Niña summer experience $+ve$ ISMR anomaly (mean and standard deviation of ISMR for those years are 0.59 and 0.35 mm d^{-1}, respectively), El Niño summers show larger scatter (mean = −0.62 mm d^{-1}, standard deviation = 0.66 mm d^{-1}). The scatters also suggest stronger droughts than

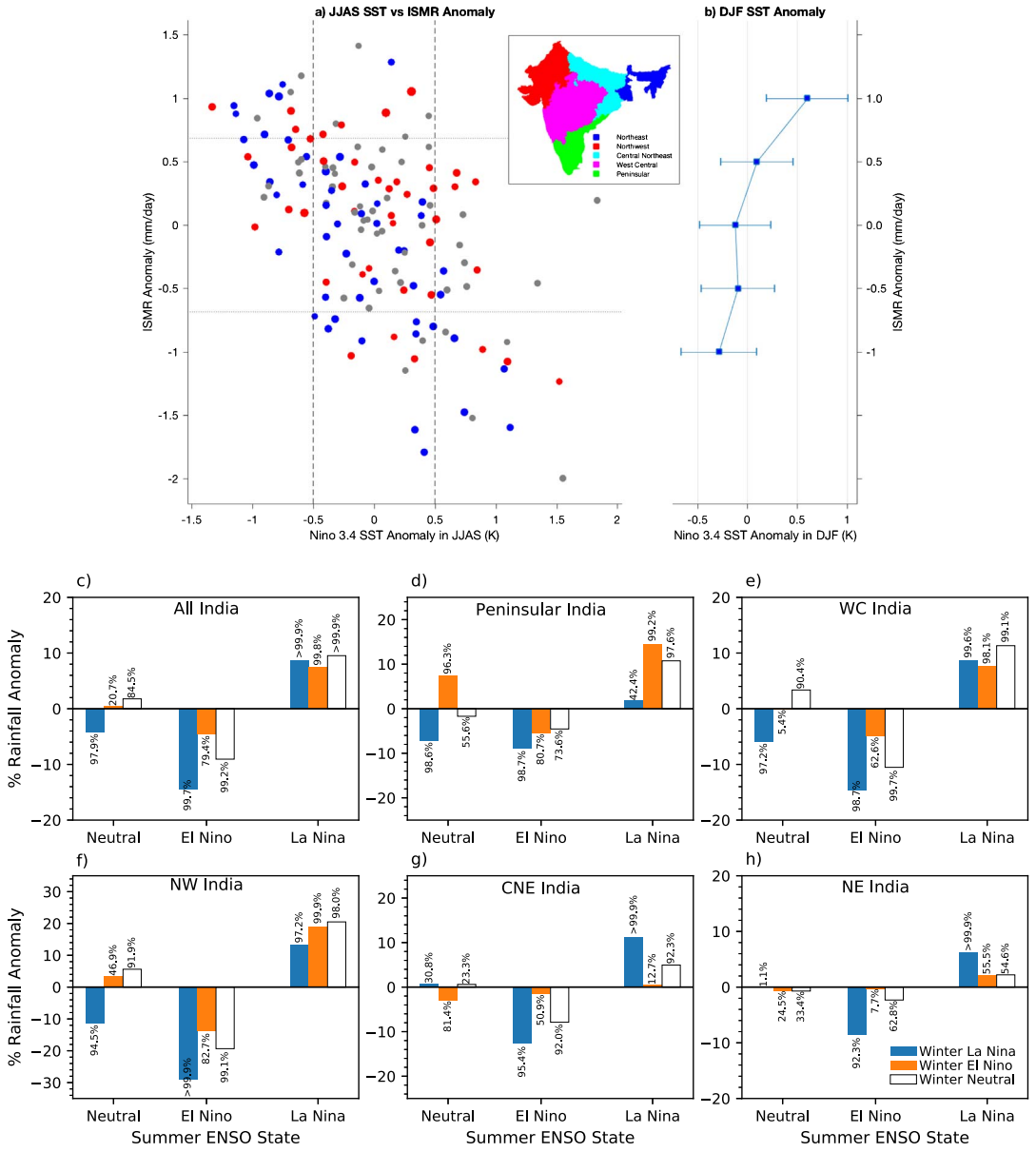

Figure 1. Relationship between ISMR and N34SST. (*a*) ISMR vs JJAS averaged N34SST anomaly during 1871–2014. The linear correlation coefficient between these two is −0.57. The red (blue) colored years correspond to positive (negative) N34SST in preceding DJF: the larger the marker, the stronger the anomaly. Only those years are colored for which the N34SST magnitude exceeds half of its interannual standard deviation in DJF. Other years are colored in gray. The two vertical lines at ±0.5 K indicate definition of La Niña, neutral and El Niño states. The two horizontal dotted lines show ± one standard deviation of ISMR, indicating thresholds for drought and flood. The color shades in inset indicate homogeneous regions to define ISMR. (*b*) DJF averaged N34SST for various ranges of ISMR anomaly (<-0.75, then every 0.5 up to 0.75 and > 0.75) during JJAS ENSO neutral years. The error bars indicate 95% confidence interval about the mean. (*c*)–(*h*) Mean rainfall composited for various states of ENSO during JJAS and the preceding DJF, over all-India (ISMR), and its five homogeneous regions. The numbers along each bar indicate the significance level at which the hypothesis that *mean ISMR anomaly equals zero* is rejected.

floods, not necessarily relating to summer El Niño. Besides, most of the variance in ISMR is noticed when JJAS N34SST is neutral. About 28% of the summer ENSO neutral years experience drought or flood (ISMR $< -10\%$ or $> +10\%$ of its long-term climatology).

The colors and size of the markers on figure 1(*a*) indicate N34SST in the preceding winter (DJF); the larger the marker, the stronger the anomaly. Note the skewed distribution of DJF N34SST along the ISMR axis. Many of the warm (cold) winters seem to be associated with increased (decreased) ISMR for a given value of N34SST in summer. This is particularly true for years when JJAS ENSO is in a state of neutral or El Niño.

Now, we identify all JJAS ENSO neutral years and calculate average N34SST in the preceding winter for different ranges of ISMR (figure 1(*b*)). This quantifies the relationship between N34SST in winter and ISMR for JJAS ENSO neutral years. It is clear that warm SST in DJF results in increased ISMR even when JJAS ENSO is neutral. This is especially true for ISMR anomalies $< -0.75\,\mathrm{mm\,d^{-1}}$ and $> 0.75\,\mathrm{mm\,d^{-1}}$. We explore this further computing conditional composites based on N34SST.

ISMR composited separately for years when JJAS ENSO is neutral, El Niño or La Niña are shown in figure 1(*c*). Even when summer ENSO is neutral, ISMR appears to be dependent of the phase of ENSO in the preceding winter. If preceding winter was La Niña, the mean of ISMR is about 4% below normal, and about 70% of those years experience $-ve$ ISMR anomaly. Although we do not include the 2017 summer season in this study, from observations we know that there were several such years in the past, including 2017 when the ISMR anomaly was close to −5% with an ENSO neutral summer that followed winter La Niña. When we compare this with winter El Niño years, summer neutral conditions of ENSO produce mostly close to normal ISMR. The hypothesis that *mean ISMR anomaly during JJAS ENSO neutral for DJF La Niña years is zero* is rejected at 97.9% significant level.

Summer El Niño conditions result in below normal ISMR. These anomalies are stronger compared to JJAS ENSO neutral years preceded by DJF La Niña, suggesting that the simultaneous impact of ENSO on ISMR is stronger than the delayed impact, and is consistent with previous findings. However, when summer El Niño was preceded by winter La Niña, the negative anomaly is more severe (mean ∼−14.5%). In contrast, summer El Niño years preceded by El Niño do not experience such large deficit in ISMR (mean ∼−5.3%). However, when El Niño is preceded by winter ENSO neutral conditions (white bars of figure 1(*c*)), the ISMR is significantly below normal. Although there are not too many years of summer El Niño preceded by winter El Niño, consistent with previous studies [32], we note that the composite N34SST in JJAS is similar for winter El Niño, La Niña and neutral states (figure S1). However, it must be kept in mind that ENSO-ISMR relationship could be non-linear and the differences seen could partly be associated with different amplitudes of the sampled events.

Summer La Niña conditions produce positive ISMR anomaly (3rd set of bars in figure 1(*c*)), again consistent with previous findings. But we do not find any significant impact of the previous winter's ENSO on ISMR during La Niña summer. However, there are large spatial differences, which are discussed later.

Figures 1(*d*)–(*h*) show that summer rainfall over southern and north-western parts of India are mostly sensitive to preceding winter ENSO condition. For example, over peninsular India, winter El Niño and La Niña years produce opposite signs of rainfall anomaly that is significant at least at the 95% level. Similarly, winter El Niño with summer La Niña produces large positive anomaly in rainfall ($>$ 15%) that is significant at the 99.2% level, and larger than for winter La Niña and neutral conditions.

The spatial patterns of JJAS mean precipitation composites based on IMD 1° × 1° observations for six different combinations of winter and summer ENSO states (of figure 1(*c*)) are shown in figure 2. Summer ENSO neutral years with preceding winter El Niño (figure 2(*a*)) are marked by negative precipitation anomaly over western and southern India. The anomalies are close to zero for summer ENSO neutral years with preceding winter El Niño (figure 2(*d*)). Similarly, summer El Niño years those come from winter La Niña (figure 2(*b*)) shows stronger negative anomalies all over the Indian region as compared to years of persisting El Niño (figure 2(*e*)). In figures 2(*c*) and (*f*) we see that previous winter El Niño or La Niña redistributes rainfall spatially during La Niña summer. While Northeast India receives more precipitation for persisting La Niña conditions (figure 2(*c*)), the transformation of El Niño to La Niña produces more precipitation over western and southern India. Differences between the composites for winter La Niña and El Niño are statistically significant over several parts of Indian land (figures S2 and S3).

Panels of figure 2(*g*) show the probability distribution of JJAS mean precipitation over five homogeneous regions of Indian summer monsoon (area weighted average of these values is the 144 year ISMR data from [26]), separately constructed for winter La Niña and El Niño, irrespective of the summer ENSO state. Over peninsular India (PEN), winter La Niña increase probability of strong and moderate drought in summer. At the same time, winter El Niño increases the probability of rainfall $>$ 1 mm d^{-1} over this region. Similarly, the probability curves for west central India (WC) and north-west India (NW) are skewed toward negative (positive) side of the distribution for La Niña (El Niño) winter, signifying the increased probability of drought (flood). On the contrary, the probability curve for precipitation over central Northeast India (CNE) is positively skewed for winter La Niña (consistent with the spatial map). The difference in summer precipitation over Northeast India (NE) between winter La Niña and El Niño is insignificant.

3.1. Mechanism

It is known that large-scale circulations associated with p_s are a dominant signature in the subtropics and midlatitudes. The subtropical high of the western North Pacific Ocean induces large anticyclonic circulation that has substantial interannual variation [33]. On the other hand, to the western side of India (over West Asia), climatological surface pressure is lower than that at the equator along the same longitude. This pressure gradient drives the strength and position of the cross-equatorial low-level winds over the Arabian Sea. Interannual variations of this gradient affect the date of the onset of the monsoon over central India [30]. Figures 3(*a*)–(*d*) show spatial variation of regression coefficients between N34SST in DJF with surface pressure (shaded) and vertically integrated moisture flux (vector) in four different seasons. In January–February (figure 3(*a*)), p_s of tropical western Pacific increases with an increase in N34SST. This is a typical response of the atmosphere during ENSO in winter [25]. Associated with this increase in p_s is

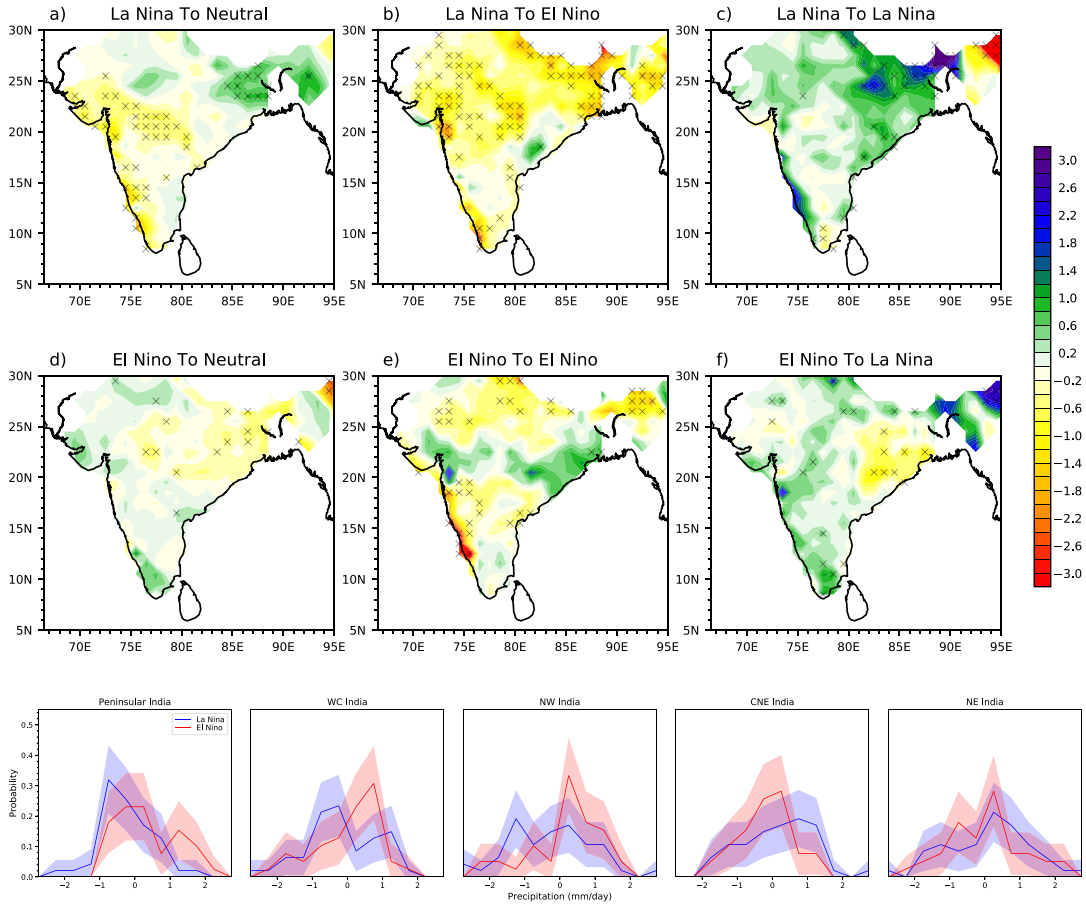

Figure 2. Spatial variation of JJAS precipitation for different winter and summer ENSO states. Panels (*a*)–(*f*) show precipitation anomaly (mm/day) composited separately for ENSO neutral, El Niño and La Niña summer with La Niña and El Niño winter. The crossed grids are regions where this anomaly is different than *zero* at least at 90% level. Panels of (*g*) show probability distribution of precipitation over five homogeneous regions of India for preceding winter La Niña (blue lines) and El Niño (red lines) conditions, irrespective of the summer ENSO state. The 90% confidence band, calculated using a binomial distribution, is shown as shades (supplementary text S1).

anomalous anticyclonic moisture flux over western Pacific and anomalous westward moisture flux over equatorial Indian Ocean. We also notice a decrease (increase) in p_s northwest of India with El Niño (La Niña) condition in winter.

In March–April (figure 3(*b*)), the equatorial western Pacific p_s anomaly weakens and is mostly centered at around 15°–20°N. The negative p_s anomaly of western Asia also weakens but its center moves southeast. In May–June (figure 3(*c*)) the high of western Pacific weakens further but extends westward and merges with the high over the Indian region. At the same time, p_s over the northern Arabian Sea and northwestern India increases. This results in the weakening of the low-level westerlies and a decrease in moisture flux to the Indian region from the Arabian Sea, consistent with [30]. This can have an impact on the onset date of the monsoon, which is discussed later. However, note that the low p_s region over 20–40 E, 30–50 N still persists, although weak. In July–August–September (figure 3(*d*)) this low p_s region moves southeast close to the Indian monsoon, strengthening the low level moisture flux through the Arabian Sea toward India. We also notice the persistence of the western North Pacific high pressure, transporting anomalous moisture toward Indian region from west. This increase (decrease) in moisture flux toward India in summer following warm (cold) N34SST of the preceding winter increases (decreases) precipitation over India, as seen in figures 1(*b*) and 2.

Composites of moisture flux are calculated for summer ENSO neutral years. Figures 3(*e*) and (*f*) show the latitudinal profile of eastward moisture flux at 70°E and 85°E, respectively, during years when summer ENSO was neutral, and composited separately for preceding winter La Niña or El Niño. At 70°E, the eastward moisture flux south of 20°N is anomalously negative in JJAS ENSO neutral years with DJF La Niña. At the same time, in DJF El Niño years the Indian region receives more moisture from the west in JJAS ENSO neutral state. These results are consistent with the p_s and moisture flux vector anomalies shown in figures 3(*c*) and (*d*). In figure 3(*f*), we find that the westward influx of moisture to the Indian region at 85°E in JJAS is higher for DJF El Niño years as compared to La Niña years. This is due to the presence of anomalous subtropical high (low) of western north Pacific, persistent from preceding winter El Niño (La Niña)

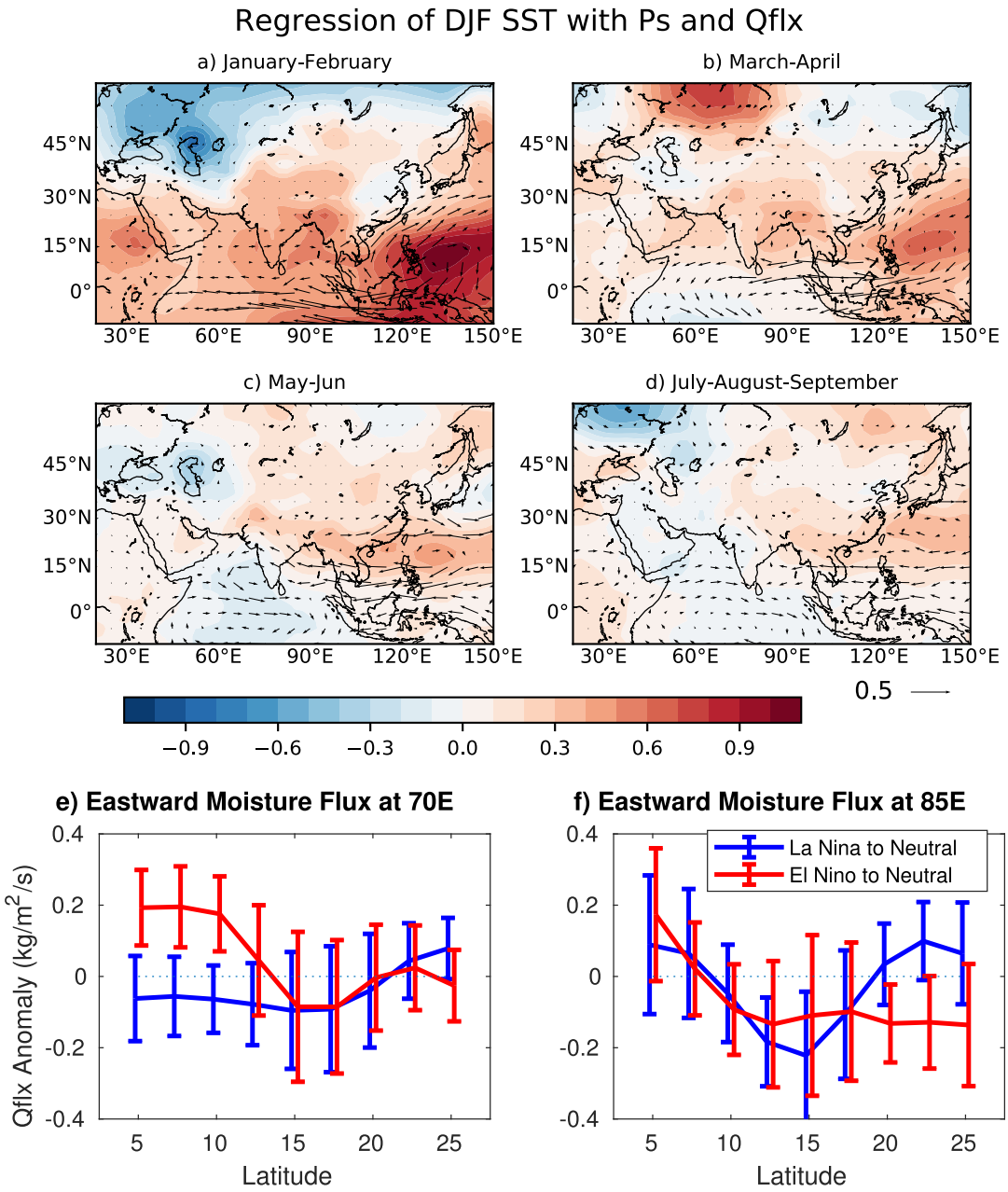

Figure 3. Relationship between p_s and DJF N34SST. Regression coefficients (hPa/K) between DJF mean N34SST with p_s (shaded) and vertically integrated moisture flux (vector) in (*a*) January–February, (*b*) March–April, (*c*) May–June, and (*d*) July–September. Panels (*e*) and (*f*) show vertically integrated moisture flux as a function of latitude along 70 E and 85 E, respectively, during ENSO neutral summer composited separately for La Niña and El Niño winter conditions, with 90% confidence band.

and associated anticyclonic (cyclonic) circulation (figure 3(*c*) and (*d*)) [25].

How do these p_s anomalies propagate in space from winter to summer? Figures 4(*a*) and (*b*) show the longitude-time evolution of monthly p_s anomaly along 20°–30°N during ENSO neutral summer, composited separately for La Niña and El Niño winters. The La Niña (El Niño) winters are associated with increased (decreased) p_s in northern subtropics. These anomalies are seasonally persistent from December to April. It is interesting to note here that during northern winter and spring, p_s anomalies are of opposite signs between 0–180°E and 0–180°W. In May, p_s anomalies become $+ve$ ($-ve$) between 0–60°E for winter La Niña (El Niño) condition. The is more prominent for winter La Niña to summer ENSO neutral years (figure 4(*a*)) for which $+ve$ p_s anomalies develop over the north and west of the Indian region and persist up to September. This could be responsible for reduced eastward moisture flux over the Arabian Sea that can affect ISMR [30].

We now analyze the time evolution and propagation of p_s anomalies for all years, averaged between 20°–30°N, from winter to summer using principal component analysis. The first mode of time-longitude evolution shows a standing wave with prominent high from 10 W to 120 E, covering the European and Asian midlatitude. The time evolution of this pattern

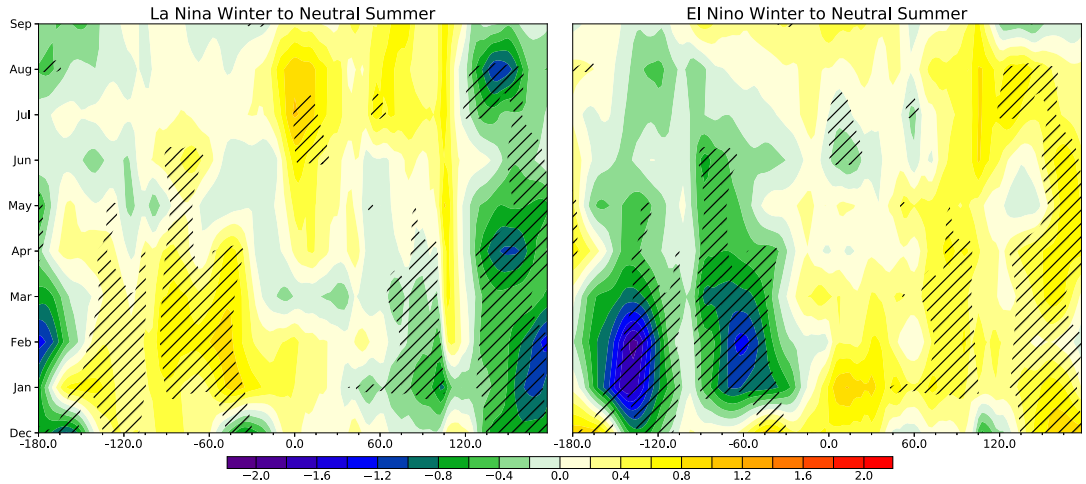

Figure 4. Zonal propagation of surface pressure anomaly. Time-longitude cross section of p_s anomaly along 20–30 N during JJAS ENSO neutral years, composited separately for preceding winter La Niña (left) and El Niño(right) conditions. The hatching shows regions where the differences in the anomalies (between winter La Niña and El Niño) are different at 90% level, calculated using a *t*-test. Thus, the hatched regions are same on both the panels.

does not show any prominent propagation in longitude direction. The associated PC shows interannual variation amid increase since 1960s and decrease after mid-1990s. We found that this PC is closely associated with the date of onset of the monsoon over peninsular India ($r = 0.44$). Note that early onset before the 1960s and delayed onset afterward is associated with this pattern of p_s. Reference [30] has shown that an increase in p_s over western Asia can delay the onset of the monsoon because of a decrease in westerly moisture flux toward India. The current finding, in addition, sheds light on the observed long-term variation of the onset over peninsular India.

The second mode (figures 5(*c*) and (*d*)) is closely associated with the winter ENSO condition ($r = 0.6$). El Niño (La Niña) decreases (increases) p_s of subtropical eastern Pacific Ocean and increases (decreases) p_s over western Pacific Ocean. The anomalies of the eastern Pacific fizzle out after winter. However, the anomalies of western Pacific associated with this principal component strengthen in northern summer. This is consistent with figure 3. The associated p_s anomalies move westward from winter to summer at a speed of about 7 degrees of longitude per month from winter to summer.

The third and fourth modes are associated with winter and summer N34SST, and their difference, although somewhat weakly. The fifth mode shows prominent eastward propagation (figures 5(*i*) and (*j*)), with speed of about 32 degrees of longitude per month. p_s anomalies of eastern Pacific Ocean in winter propagate eastward and become more prominent between 0°–120°E after April. At the same time, p_s anomalies of central Pacific Ocean (180°–240°E) propagate eastward and appear over western Pacific Ocean by JJAS. A positive (negative) value of the associated PC time series results in a decrease (increase) in p_s over west Asia (west Pacific Ocean) that increase (decrease) moisture flux toward the Indian region. This increases precipitation over India, as seen by the correlation between this PC time series with ISMR ($r = 0.48$). Note that this value of correlation coefficient between τ_5 and ISMR is close to that between ISMR and JJAS N34SST (-0.57).

4. Discussions

In this study, we quantify the relative impacts of ENSO in summer and in the preceding winter on summer monsoon rainfall over India. We focus on years of ENSO neutral summer since interannual variations of ISMR during those years are least understood. The primary findings are:

a. Winter La Niña reduces following summer monsoon rainfall over India by about 4% even during ENSO neutral summer. The partial correlation between DJF N34SST and ISMR, after regressing out the effect of JJAS N34SST on ISMR is 0.27 (significant at 95% level). These results are consistent with previous findings [21] that use the tendency of Darwin surface pressure. However, the present study uses SST that has higher auto-correlation in time than surface pressure.

b. This impact of preceding winter La Niña is strongest during El Niño summer (ISMR anomaly about −14.5%, as opposed to −5.3% for a persistent El Niño), increasing the probability of severe drought. This is reported for the first time and would have high socio-economic importance.

c. The western and southern parts of Indian land are most prone to reduced precipitation when the preceding winter was La Niña. Such spatial variations of the impact of winter ENSO is also reported for the first time.

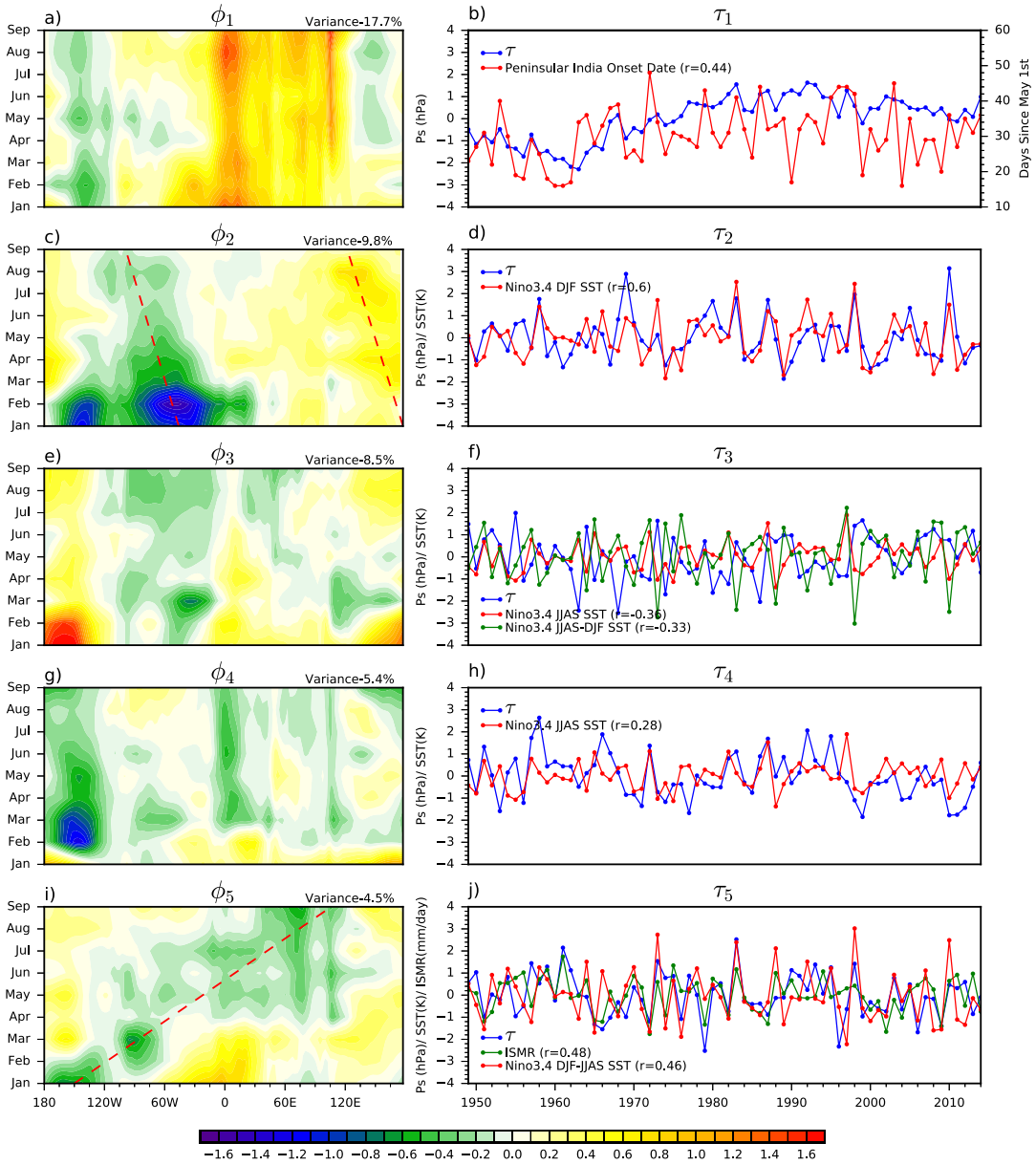

Figure 5. Seasonal evolution of p_s anomaly along Northern Hemisphere subtropics. First five empirical orthogonal function (EOF; ϕ) patterns (left panels) and principal component (PC; τ) time series (right panels, in hPa) of p_s anomaly averaged between 20–30 N. The right side panels also show few other variables correlated to the PC time series. The variance explained by these components are indicated at top right corner of EOF panels. The dotted lines on (*c*) and (*i*) indicate the spatial evolution/propagation of p_s from winter to summer associated with winter (DJF) N34SST and its change from winter to summer (JJAS). All correlation values (r) greater than 0.24 are significant at 95% level. Cross correlation between different PCs and other parameters are in table S3.

d. As ENSO weakens after the strongest amplitude in winter, surface pressure anomalies propagate along northern subtropical longitude, both toward east (faster) and west (slower). This modulates surface pressure over west Asia and west Pacific Ocean during May–September, impacting moisture transport through the Arabian Sea and the Bay of Bengal. The anomalous moisture transport modifies monsoon precipitation over India.

The delayed impact of El Niño on the Indian Ocean region is known to be through the thermal capacitor effect [34]. The continued warming signal of the tropical Indian Ocean after a strong El Niño event during winter could change the climate around this region [35, 36], especially weakening monsoon circulation. Our results show that the effect of preceding winter La Niña on ISMR is more as compared to that of preceding winter El Niño. Composite plots of seasonal evolution of global SST, done separately for winter La Niña and El Niño (supplementary figures 2 and 3) show that while the Indian Ocean is warmer during JJAS for preceding winter El Niño, SST is close to normal for winter La Niña years. In other words, the thermal capacitor

effect (in this case cooling) is not observed for La Niña to neutral years. The increased SST over Indian Ocean for summers preceded by El Niño could reduce the impact of mid-latitude p_s anomalies on monsoon rainfall over India, as was seen in figure 1(*c*).

5. Conclusion

This study, for the first time, quantifies the precipitation anomaly over different regions of India resulting from combined states of ENSO in winter and summer. The results not only highlight this spatial variation of precipitation, but also underlines the asymmetry of the impact of El Niño and La Niña of winter and summer on the summer monsoon. The method of identifying modes of time-longitude evolution of surface pressure decomposed standing anomalies from propagations without pre-assuming periodicity. This method and other findings could be used for the evaluation of numerical models employed for seasonal prediction of the monsoon, which normally show poor skill in capturing the impact of ENSO on ISMR and its spatial variations.

Acknowledgments

The author acknowledges the support of the Department of Science and Technology, India under grant DST/CCP/NCM/77/2017. The author also thanks IMD, IITM and NCEP for constructing and distributing invaluable data sets used in this study, and J Srinivasan and S Gadgil for discussions. The support of Ishwar M Bhat in analysis is greatly appreciated. The author thanks two anonymous reviewers for thorough and important comments.

ORCID iDs

Arindam Chakraborty https://orcid.org/0000-0002-4288-0216

References

[1] Gadgil S and Kumar K R 2006 The Asian monsoon—agriculture and economy *The Asian Monsoon* (Berlin: Springer) pp 651–83
[2] Revadekar J and Preethi B 2012 Statistical analysis of the relationship between summer monsoon precipitation extremes and foodgrain yield over India *Int. J. Climatol.* **32** 419–29
[3] Mooley D A and Parthasarathy B 1984 Fluctuations in All-India summer monsoon rainfall during 1871–1978 *Clim. Change* **6** 287–301
[4] Yasunari T and Seki Y 1992 Role of the Asian monsoon on the interannual variability of the global climate system *J. Meteorol. Soc. Jpn. Ser II* **70** 177–89
[5] Wainer I and Webster P J 1996 Monsoon/El Niño-Southern Oscillation relationships in a simple coupled ocean-atmosphere model *J. Geophys. Res. Oceans* **101** 25599–614
[6] Tsonis A A, Swanson K and Kravtsov S 2007 A new dynamical mechanism for major climate shifts *Geophys. Res. Lett.* **34** L13705
[7] de Viron O, Dickey J O and Ghil M 2013 Global modes of climate variability *Geophys. Res. Lett.* **40** 1832–7
[8] Krishnamurti T N 1971 Observational study of the tropical upper tropospheric motion field during the northern Hemisphere summer *J. Appl. Meteorol.* **10** 1066–96
[9] Krishnamurti T N 1971 Tropical east-west circulations during the northern summer *J. Atmos. Sci.* **28** 1342–7
[10] Walker G T 1925 Correlatoin in seasonal variations of variasions of weather–A further study of world weather 1 *Month. Wea. Rev.* **53** 252–4
[11] Kumar K K, Rajagopalan B, Hoerling M, Bates G and Cane M 2006 Unraveling the mystery of Indian monsoon failure during El Niño *Science* **314** 115–9
[12] Hoskins B J and Karoly D J 1981 The steady linear response of a spherical atmosphere to thermal and orographic forcing *J. Atmos. Sci.* **38** 1179–96
[13] Shaman J and Tziperman E 2007 Summertime ENSO–North African–Asian Jet teleconnection and implications for the Indian monsoons *Geophys. Res. Lett.* **34** L11702
[14] Barnett T P 1985 Variations in near-global sea level pressure *J. Atmos. Sci.* **42** 478–501
[15] Yasunari T 1987 Global structure of the El Niño/Southern Oscillation *J. Meteorol. Soc. Jpn Ser II* **65** 81–102
[16] Huang R and Wu Y 1989 The influence of ENSO on the summer climate change in China and its mechanism *Adv. Atmos. Sci.* **6** 21–32
[17] Shen S and Lau K M 1995 Biennial Oscillation associated with the east Asian summer monsoon and tropical sea surface temperatures *J. Meteorol. Soc. Jpn Ser II* **73** 105–24
[18] Chang C P, Zhang Y and Li T 2000 Interannual and interdecadal variations of the east Asian summer monsoon and tropical pacific SSTs. Part I: roles of the subtropical ridge *J. Clim.* **13** 4310–25
[19] Wu R and Wang B 2002 A contrast of the East Asian summer monsoon-ENSO relationship between 1962–77 and 1978–93 *J. Clim.* **15** 3266–79
[20] Shukla J and Paolino D A 1983 The southern Oscillation and long-range forecasting of the summer monsoon rainfall over India *Month. Wea. Rev.* **111** 1830–7
[21] Shukla J and Mooley D A 1987 Empirical prediction of the summer monsoon rainfall over India *Month. Wea. Rev.* **115** 695–703
[22] Rajeevan M, Pai D, Kumar R A and Lal B 2007 New statistical models for long-range forecasting of southwest monsoon rainfall over India *Clim. Dyn.* **28** 813–28
[23] Hastenrath S 1988 Prediction of Indian monsoon rainfall: further exploration *J. Clim.* **1** 298–304
[24] Hastenrath S and Greischar L 1993 Changing predictability of Indian monsoon rainfall anomalies? *J. Earth Syst. Sci.* **102** 35–47
[25] Wang B, Wu R and Fu X 2000 Pacific-East Asian teleconnection: how does ENSO affect East Asian climate? *J. Clim.* **13** 1517–36
[26] Parthasarathy B, Munot A A and Kothawale D R 1994 All-India monthly and seasonal rainfall series: 1871–1993 *Theor. Appl. Climatol.* **49** 217–24
[27] Rajeevan M N, Bhate J, Kale J D and Lal B 2006 High resolution daily gridded rainfall data for the Indian region: analysis of break and active monsoon spells *Curr. Sci.* **91** 296–306
[28] Rayner N A 2003 Global analyses of sea surface temperature, sea ice, and night marine air temperature since the late nineteenth century *J. Geophys. Res.* **108** 4407
[29] Kalnay E *et al* 1996 The NCEP/NCAR 40 year reanalysis project *Bull. Am. Meteorol. Soc.* **77** 437–71
[30] Chakraborty A and Agrawal S 2017 Role of west Asian surface pressure in summer monsoon onset over central India *Environ. Res. Lett.* **12** 074002–9

[31] Messié M and Chavez F 2011 Global modes of sea surface temperature variability in relation to regional climate indices *J. Clim.* **24** 4314–31
[32] Santoso A, McPhaden M J and Cai W 2017 The defining characteristics of ENSO Extremes and the strong 2015/2016 El Niño *Rev. Geophys.* **55** 1079–129
[33] Wu B, Li T and Zhou T 2010 Asymmetry of atmospheric circulation anomalies over the western North Pacific between El Niño and La Niña *J. Clim.* **23** 4807–22
[34] Xie S P *et al* 2009 Indian ocean capacitor effect on indo–Western Pacific climate during the summer following El Niño *J. Clim.* **22** 730–47
[35] Kug J S *et al* 2006 Role of the ENSO–Indian Ocean coupling on ENSO variability in a coupled GCM *Geophys. Res. Lett.* **33** L09710
[36] Herold N and Santoso A 2017 Indian Ocean warming during peak El Niño cools surrounding land masses *Clim. Dyn.* (https://doi.org/10.1007/s00382-017-4001-6)